

Rabi oscillation induced π -phase flip in an unbalanced Ramsey atom interferometer

R. B. Li,^{1,2,*} Z. W. Yao,^{1,2} K. Wang,^{1,2,3} S. B. Lu,^{1,2,3} L. Cao,^{1,2,3} J. Wang,^{1,2,†} and M. S. Zhan^{1,2,‡}

¹State Key Laboratory of Magnetic Resonance and Atomic and Molecular Physics,
Wuhan Institute of Physics and Mathematics, Chinese Academy of Sciences, Wuhan 430071, China

²Center for Cold Atom Physics, Chinese Academy of Sciences, Wuhan 430071, China

³University of Chinese Academy of Sciences, Beijing 100049, China

(Dated: July 5, 2016)

We present an observation of zero to π phase flips induced by Rabi oscillation in an unbalanced Ramsey atom interferometer. The phase shift and visibility are experimentally investigated by modulating either the polarization or duration of Raman lasers, and they are well explained by a theoretical model. In an atom interferometer, the π -phase flips are caused not only by the sign of Rabi frequency but also by the Rabi oscillation. Considering the π -phase flips, we propose the composite-light-pulse sequences for realizing the large-momentum-transfer beam splitter and mirror, which have the high immunity to the external phase noise in building the cold atom interferometer.

PACS numbers: 37.25.+k, 03.75.Dg, 32.80.Qk, 03.65.Vf

Since the light-pulse atom interferometer was demonstrated [1], it has been applied in many scientific and technical fields, such as measurements of the gravitational constant [2, 3] and the fine structure constant [4, 5], test of the weak equivalence principle [6–8], and inertial instruments of atomic gyroscopes [9–11] and atomic gravimeters [12, 13]. In addition, atom interferometers used in test of the general relativity [14–16] and detection of the gravitational wave [17–20], were even proposed. The sensitivity of atom interferometer can be improved by enlarging its interferometric area. To make a large area, many techniques including the multi-light-pulse sequence [21], sequential multiphoton Bragg diffraction [22–24] and frequency-swept Raman adiabatic passage [25] were applied. On the other hand, the sensitivity can be improved by suppressing the phase noise during the atomic free evolution. For this purpose, the double diffraction technique was developed [26, 27].

The beam splitter and mirror are the central elements of atom interferometer, and their phase noise limits the quantum behavior determined sensitivity and stability. To further improve the sensitivity of atom interferometer, it is essential to synchronously enlarge the interferometric area and suppress the phase noise. Thus the composite-light-pulse (CLP) sequences were used to create the large-momentum-transfer (LMT) beam splitter and mirror in the atom interferometer [28]. In the CLP sequences based atom interferometer, the external technical noise during the intervals of the atomic free evolution, was greatly suppressed due to the atoms stayed in the same states. However, the phase noise in the CLP sequences can not be suppressed during the atomic wave-packet manipulations. Therefore, it is important to simultaneously suppress the phase noise in the CLP sequences and during

the atomic free evolution. Recently, we found a π -phase flip when the polarization, intensity or duration of Raman lasers were modulated in the atom interferometer, which is useful for building the CLP sequences.

In this paper, we design and implement an experiment to quantitatively investigate the phase shift induced by the Rabi oscillation in the atom interferometer. The zero to π phase flips are observed in an unbalanced Ramsey atom interferometer by modulating the polarization and duration of Raman lasers, and they are well explained by the sign of Rabi frequency and the Rabi oscillation. Considering the π -phase flips between two consecutive Raman transitions, the new CLP sequences are proposed for building the LMT beam splitter and mirror. The phase noise is discussed, and it can be cancelled in the CLP sequences and during the atomic free evolution. These CLP sequences can be used to build the low-phase-noise large-area atom interferometer, and it is important to improve the sensitivity and stability of atom interferometer.

The experiment is performed in the unbalanced Ramsey interferometer where the atoms are coherently manipulated by two asymmetrical Raman pulses [29]. The experimental arrangement (top view) is shown in Fig. 1 (a). The atoms (^{85}Rb) are trapped in a magneto-optical trap (MOT). Then they are launched along a parabolic trajectory, with an initial velocity of 2.5 m/s and an angle of 14.0° with respect to the gravity. The polarization gradient cooling is applied when the atoms are accelerating in the MOT. Thus, an atom fountain is built with the low temperature ($<5\text{ }\mu\text{K}$). When cold atoms are propagating from the MOT to probe regions, they are pumped to the state $|5S_{1/2}, F=2\rangle$. Two pairs of Raman lasers, with a time interval of $T=50\text{ ms}$, are co-propagating along the magnetic field B (100 mG). The magnetic field B_0 is adjusted to cancel the residual magnetic field [30]. The Raman lasers with frequency difference of 3.04 GHz are generated from the ± 1 order diffracted lights of an acousto-optic modulator (1.52 GHz) [31]. The Raman lasers couple two ground states $|F=2, m_F=0\rangle$ and $|F=3, m_F=0\rangle$ with the excited states $|5P_{3/2}\rangle$, where

*rbli@wipm.ac.cn

†wangjin@wipm.ac.cn

‡mszhan@wipm.ac.cn

the one-photon detuning is 1.5 GHz. When the atoms are operated by the Raman lasers, Raman transitions are observed and Raman pulses are defined by the Rabi frequency and duration of Raman lasers. When the atoms in the initial state $|F = 2, m_F = 0\rangle$ are manipulated by two symmetrical or asymmetrical Raman pulses, the balanced and unbalanced Ramsey fringes are observed by measuring the population in the state $|F = 3, m_F = 0\rangle$ using the laser-induced fluorescence signal.

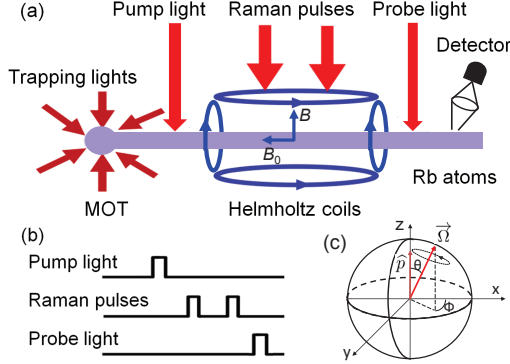


FIG. 1: (Color online) Experiment setup (a), timing sequences (b) and Bloch sphere depiction (c). Cold atoms are propagating from the MOT to the probe region. The atoms are manipulated by two pairs of Raman lasers with a time interval of T . Ramsey fringes are observed by measuring the population using the laser-induced fluorescence signal.

With the timing sequences in Fig. 1 (b), Ramsey fringes are obtained by scanning the phase difference of Raman lasers, as shown in Fig. 2. A typical balanced Ramsey fringe is observed with two symmetrical $\pi/2$ pulses of (σ^+, σ^+) and (σ^+, σ^+) (black squares), and an unbalanced Ramsey fringe is also observed with two asymmetrical $\pm\pi/2$ pulses of (σ^+, σ^+) and (σ^-, σ^-) (red circles). There is a π -phase shift when the polarization of the second pulse is rotated from (σ^+, σ^+) to (σ^-, σ^-) . In the same way, the π -phase shift is also observed when the polarization of the first pulse is rotated from (σ^+, σ^+) to (σ^-, σ^-) while the polarization of the second pulse is maintained in (σ^+, σ^+) . The phase shift and visibility are quantitatively investigated when the polarization is continuously rotated in one cycle. Here, the first $\pi/2$ pulse stays in (σ^+, σ^+) , and the polarization of the second $\pi/2$ pulse is rotated from $\beta_2 = 0$ to 360° by rotating the polarization axis of the $\lambda/4$ wave plate from $\beta'_2 = 0$ to 180° [32]. Similar to Fig. 2, the Ramsey fringes are obtained and fitted by sine wave functions. Fig. 3 shows the phase shift (black crosses) and the visibility (red stars) when the polarization of the second Raman pulse is rotated from $\beta_2 = 0$ to 360° . In Fig. 3 (black crosses), the π -phase flip is observed by rotating the polarization, which is similar to the results obtained by rotating the magnetic field [33, 34]. In their experiments, the observed π -flipped phase was interpreted as a geometric phase [33], caused by a parity-dependent phase factor of $(-1)^F$ for $m = 0$

spin states [35], and it was also explained by an opposite sign between two transition amplitudes [34].

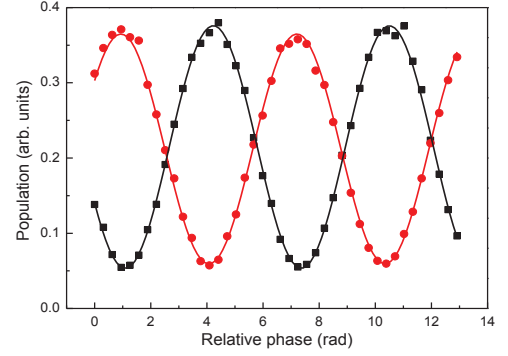


FIG. 2: (Color online) Observed Ramsey fringes with two Raman pulses of (σ^+, σ^+) and (σ^+, σ^+) (black squares), while (σ^+, σ^+) and (σ^-, σ^-) (red circles). There is a π -phase shift when the polarization is rotated from (σ^+, σ^+) to (σ^-, σ^-) .

The above results can be well explained by the theoretical equations of the unbalanced Ramsey interferometer. We consider a pair of Raman lasers couple two ground states $|a\rangle$ and $|b\rangle$ with an excited state $|i\rangle$. The first $\pi/2$ pulse takes the initial state $|a\rangle$ into a superposition state $(|a\rangle + |b\rangle)/\sqrt{2}$. After a free evolution time of T , the second arbitrary pulse then recombines the atomic wave packets. Finally, the probability amplitude of the state $|b\rangle$ is obtained by [36, 37]

$$b = \frac{1}{\sqrt{2}} \left[\cos \frac{\Omega_2 \tau_2}{2} e^{-i(\omega_2 T - \phi_1)} + \sin \frac{\Omega_2 \tau_2}{2} e^{-i(\omega_1 T - \phi_2)} \right] \quad (1)$$

where, ϕ_j is the phase of the j th Raman pulse, Ω_j and τ_j are the Rabi frequency and the pulse duration of the j th Raman interactions, and ω_1 and ω_2 are the perturbed frequencies of two ground states. The population probability of the state $|b\rangle$ is written as

$$bb^* = \frac{1}{2} \{ 1 + \sin(\Omega_2 \tau_2) \cos[(\omega_2 - \omega_1)T + \phi_2 - \phi_1] \} \quad (2)$$

where, $|\sin(\Omega_2 \tau_2)|$ is the visibility. Its behavior can be visually depicted on a Bloch sphere [38, 39] as shown in Fig. 1 (c). For an given angle β_2 , the input polarization has to be transformed into a coordinate system along the magnetic field B using a rotation matrix $D_{QQ'}^{(K)}$, where K is multiplicity and Q is $m_F - m_{F'}$ [40]. For $K = 1$ and $Q = 0$, the effective Rabi frequency is given by [30]

$$\Omega_2(\beta_2) = \frac{|e|^2 \varepsilon \xi}{4 \hbar^2 \Delta} \sum_i \langle b | r_q | i \rangle \langle i | r_p | a \rangle \cos \beta_2 \quad (3)$$

where, Δ is the one-photon detuning, $\langle b | r_q | i \rangle \langle i | r_p | a \rangle$ is the reduced matrix element of two-photon Raman transitions, and ε, ξ are the amplitudes of two Raman laser fields, respectively. When the polarization or magnetic field is rotated as β_2 , the sign of $\Omega_2(\beta_2)$ depends on the

sign of $\cos \beta_2$ term in Eq.(3). The π -phase flip is caused by the positive or negative sign of $\sin(\Omega_2 \tau_2)$ term in Eq.(2). The π -phase flip observed with the polarization rotated in Figs.2 and 3 (black crosses) and the magnetic field rotated in Refs.[33, 34] can be better explained by the opposite sign of Rabi frequency rather than by the geometric phase. The π -phase flip caused by the negative sign of transition amplitude is confirmed by modulating the polarization of Raman lasers. Due to two $\pi/2$ Raman pulses initially applied for $\beta_2 = 0$, the visibility can be rewritten as a function of $|\sin(\frac{\pi}{2} \cos \beta_2)|$, according to Eqs.(2) and (3), when β_2 is rotated. The experimental result (red stars) is well matched with the theoretical model (red solid curve) as shown in Fig.3.

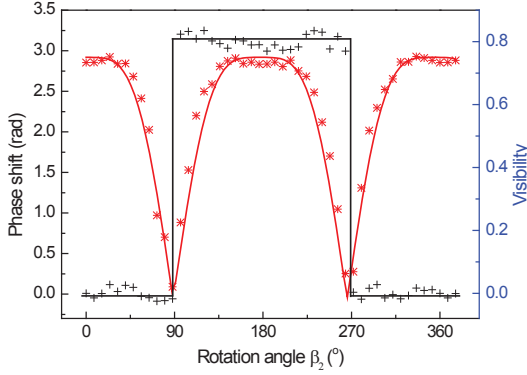


FIG. 3: (Color online) Phase shift (black crosses) and visibility (red stars) as a function of the polarization rotation angle β_2 . They are fitted by the theoretical model (solid curves).

The phase shift and visibility are investigated by modulating the pulse duration (τ_2). In the experiment, two pulses of (σ^+, σ^+) and (σ^+, σ^-) with the same Rabi frequencies ($\Omega_1 = \Omega_2$) are co-propagating along the magnetic field B . After the atoms are prepared to the coherent superposition state by the first pulse ($\Omega_1 \tau_1 = \pi/2$), they are manipulated by the second pulse whose duration is increased from $\tau_2 = 0$ to $160 \mu\text{s}$. For the first time, the Rabi oscillation induced π -phase flip is experimentally observed by modulating the duration as shown in Fig.4 (black crosses). When the duration is increased, the Raman pulse is equivalent to a combination of two Raman pulses. For example, the second pulse (for $\Omega_2 \tau_2 = 3\pi/2$) is equivalent to the combination of π and $\pi/2$ pulses. The former exchanges the population between two coherent states, and the latter recombines the atomic wave packets. Therefore, this π -phase flip can be well explained by the population exchanges between two coherent states. For the different durations, the visibility is shown in Fig.4 (red stars). From Eq.(2), the visibility should be maximum for $\Omega_2 \tau_2 = \pm M\pi/2$ (M is an odd number), and Ramsey fringes are vanished for $\Omega_2 \tau_2 = \pm N\pi/2$ (N is an even number). The maximum visibility is observed for $\tau_2 = 40 \mu\text{s}$ ($\Omega_2 \tau_2 = \pi/2$). The Ramsey fringes are nearly disappeared for $\tau_2 = 80 \mu\text{s}$ ($\Omega_2 \tau_2 = \pi$) and $\tau_2 = 160 \mu\text{s}$

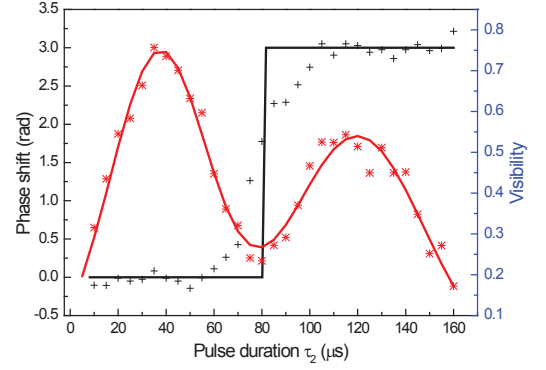


FIG. 4: (Color online) Phase shift (black crosses) and visibility (red stars) as a function of the pulse duration τ_2 . There is a π -phase flip when the pulse duration is $80 \mu\text{s}$.

($\Omega_2 \tau_2 = 2\pi$) because the atomic wave packets are not recombined. Due to the atomic velocity distribution, the decoherence is caused by the spatial intensity variation and wave front distortion of Raman lasers. The visibility for $\tau_2 = 120 \mu\text{s}$ ($\Omega_2 \tau_2 = 3\pi/2$) is less than that for $\tau_2 = 40 \mu\text{s}$. The visibility is decreased for other durations because of the partial recombination of wave packets, which is consistent with the function of $|\sin(\Omega_2 \tau_2)|$.

In above experiments, the observed π -phase flips arise from the positive or negative sign of $\sin(\Omega_2 \tau_2)$ term in Eq.(2). This behavior can be visualized on the Bloch sphere as shown in Fig.1 (c). The drive field ($\vec{\Omega}$) is rotated at a polar angle ($\theta = \Omega\tau$) when the Raman pulse is applied. The first pulse ($\theta_1 = \pi/2$) drags the Bloch vector \hat{p} at the positive z -axis into the x - y plane. After the integration time T , \hat{p} is then rotated at $\theta_2 = \Omega_2 \tau_2$ on the Bloch sphere when the second pulse is applied. The azimuthal angle ($\Phi = (\omega_2 - \omega_1)T + \phi_2 - \phi_1$) is rotated around z -axis by scanning the phase difference of the Raman lasers and it is same for each Ramsey fringe due to the cancellation of the ac Stark shift [41] and the synchronous rotation of polarizations [42]. The projection of \hat{p} onto the z -axis, $\sin \theta_2$, gives the population difference, which can depict the phase and visibility of the fringe. When β_2 is rotated, an elliptical polarization is equivalent to a combination of linear and circular polarizations. Because the two-photon transition probability induced by the linear polarization can be neglected for the large one-photon detuning, the second pulse is equivalent to (σ^+, σ^+) or (σ^-, σ^-) . The signs between two Rabi frequencies are opposite for (σ^+, σ^+) and (σ^-, σ^-) . For the positive or negative Rabi frequency, \hat{p} is projected on the negative or positive z -axis, which explains the π -phase flips in Fig.3 (black crosses). When τ_2 is increased, \hat{p} is rotated from the x - y plane to the negative z -axis. \hat{p} is projected on the negative z -axis when θ_2 is changed from zero to π , while it is projected on the positive z -axis when θ_2 is changed from π to 2π . Thus the π -phase flip is observed as shown Fig.4 (black crosses). The visibility is maximum when \hat{p} is parallel to z -axis, and the

fringe is disappeared when \hat{p} is vertical to z -axis.

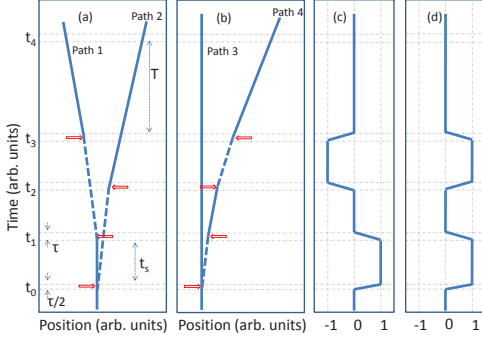


FIG. 5: (Color online) A space-time diagram of the LMT beam splitter for symmetric (a) and asymmetric (b) CLP sequences as described in Refs.[19, 28], and the corresponding sensitivity functions with (c) and without (d) considering the Rabi oscillation and sign induced π -phase flips. The sensitivity functions are calculated by the theoretical model in Ref.[43]

When the CLP sequences are applied to build the LMT beam splitter and mirror in atom interferometers, the π -phase flip modulated by the sign of Rabi frequency or the Rabi oscillation is useful for cancelling the slow varying phase noise. We discuss the phase noise in the CLP sequences composed of several rapid-succession Raman pulses, where a pair of Raman lasers are counter-propagating for the larger momentum transfer. Fig.5 (a) shows a LMT beam splitter of the symmetric CLP sequence, but four pulses are applied instead of two pulses in Ref.[28]. Fig.5 (b) shows a LMT beam splitter of the asymmetric CLP sequence as proposed in Ref.[19]. At the time t_0 , the atoms in the initial state $|a\rangle$ are split into the states $|a\rangle$ and $|b\rangle$ by the first $\pi/2$ pulse. From t_1 to t_3 , three π pulses alternately manipulate the states of atoms in the path 1 or 2 as shown in Fig.5 (a), while they only manipulate the states of atoms in the path 4 as shown in Fig.5 (b). Due to the wave vectors reversed (red double arrows), the $8\hbar k$ LMT beam splitters can be built with the symmetric and asymmetric CLP sequences.

When the pulse duration (τ) is 10 μs and the dark time (t_s) is 20 μs [28], the LMT beam splitters of the symmetric and asymmetric CLP sequences can be realized in 100 μs (from t_0 to t_3). The sensitivity functions are calculated by the theoretical model [43]. Fig.5 (c) plots the sensitivity function of the symmetric CLP sequence in Fig.5 (a). Fig.5 (d) is the sensitivity function of the asymmetric CLP sequence in Fig.5 (b). The atoms always stay in the same state $|a\rangle$ (solid lines) or $|b\rangle$ (dashed lines) during the time intervals of $[t_1 : t_2]$ and $[t_3 : t_4]$. The atom interferometer has a high immunity to the phase noise in the above time intervals. We discuss

the phase in the time intervals of $[t_0 : t_1]$ and $[t_2 : t_3]$. Due to the fact that the Rabi oscillation induced π -phase flip causes the opposite phase shifts between $[t_0 : t_1]$ and $[t_2 : t_3]$ in the symmetric CLP sequence, the phase noise (< 10 kHz) is cancelled. However, the phase noise is accumulated in the asymmetric CLP sequence. When the polarizations of Raman lasers are half-rotated at t_2 [44], the sign induced π -phase flip is introduced, and the sensitivity function is changed from Fig.5 (d) to Fig.5 (c). Thus, the phase noise (< 10 kHz) in the asymmetric CLP sequence is also cancelled because there are the opposite phase shifts between $[t_0 : t_1]$ and $[t_2 : t_3]$. The LMT beam mirrors of the symmetric and asymmetric CLP sequences can be built, and the phase noise (< 10 kHz) can also be cancelled by the same ways. At the same time, the atoms stay in the same state during the atomic free evolution (i.e., solid lines from t_3 to t_4). Thus, the slow varying phase noise both in and between the LMT beam splitters and mirrors can be simultaneously cancelled. The atom interferometer may be not limited by the classical behavior, such as the phase shift of Raman lasers caused by the temperature drift, which is important for improving the sensitivity and especially for the stability of atom interferometer.

In conclusion, the Rabi oscillation induced phase flip is observed for the first time. The π -phase flip caused by the negative sign of transition amplitude is confirmed. The π -phase flips observed by modulating the polarization and duration of Raman lasers in this work and by rotating the magnetic field in Refs.[33, 34], are well explained by a universal theoretical model. They arise from the positive or negative sign of $\sin(\Omega_2\tau_2)$ term in Eq.(2), which are visually depicted on the Bloch sphere. The CLP sequences based LMT beam splitters and mirrors are proposed for building the low-phase-noise large-area atom interferometer. Importantly, the slow varying phase noise both in and between the LMT beam splitters and mirrors can be simultaneously cancelled. Furthermore, fringes can be obtained by varying the intensity or duration of Raman lasers. The CLP sequences can also be depicted on the Bloch sphere, and they may be optimized by controlling the polar angle and azimuthal angle on the Bloch sphere. The influence of atomic velocity distribution can be decreased in the ultracold atom interferometer. This work has the potential application in atom interferometers, and it is important for developing the ultra-sensitivity atom interferometer.

We acknowledge the financial support from the National Natural Science Foundation of China under Grant Nos. 11004227 and 91536221, and funds of Youth Innovation Promotion Association of Chinese Academy of Sciences. We also thank X. W. Guan and J. Luo from WIPM, L. Deng from NIST for helpful suggestions and comments.

-
- [1] M. Kasevich, and S. Chu, Atomic interferometry using stimulated Raman transitions, *Phys. Rev. Lett.* 67, 181 (1991).
- [2] J. B. Fixler, G. T. Foster, J. M. McGuirk, and M. A. Kasevich, Atom interferometer measurement of the Newtonian constant of gravity, *Science*, 315, 74 (2007).
- [3] G. Rosi, F. Sorrentino, L. Cacciapuoti, M. Prevedelli and G. M. Tino, Precision measurement of the Newtonian gravitational constant using cold atoms, *Nature*, 510, 518 (2014).
- [4] D. S. Weiss, B. C. Young, and S. Chu, A precision measurement of \hbar/m Cs based on photon recoil using laser cooled atoms and atom interferometry, *Appl. Phys. B-Lasers Opt.*, 59 217 (1994).
- [5] R. Bouchendira, P. Clade, S. Guellati-Khelifa, F. Nez, and F. Biraben, New determination of the fine structure constant and test of the quantum electrodynamics, *Phys. Rev. Lett.* 106, 080801 (2011).
- [6] D. Schlippert, J. Hartwig, H. Albers, L. L. Richardson, C. Schubert, A. Roura, W. P. Schleich, W. Ertmer, and E. M. Rasel, Quantum test of the universality of free fall, *Phys. Rev. Lett.* 112, 023002 (2014).
- [7] M. G. Tarallo, T. Mazzoni, N. Poli, D. V. Sutyryn, X. Zhang, and G. M. Tino, Test of Einstein equivalence principle for 0-spin and half-integer-spin Atoms: Search for spin-gravity coupling effects, *Phys. Rev. Lett.* 113, 023005 (2014).
- [8] L. Zhou, S. T. Long, B. Tang, X. Chen, F. Gao, W. C. Peng, W. T. Duan, J. Q. Zhong, Z. Y. Xiong, J. Wang, Y. Z. Zhang, and M. S. Zhan, Test of equivalence principle at 10^{-8} level by a dual-species double-diffraction Raman atom interferometer, *Phys. Rev. Lett.*, 115, 013004 (2015).
- [9] B. Canuel, F. Leduc, D. Holleville, A. Gauguier, J. Fils, A. Virdis, A. Clairon, N. Dimarcq, C. J. Borde, A. Landragin, and P. Bouyer, Six-axis inertial sensor using cold-atom interferometry, *Phys. Rev. Lett.* 97, 010402 (2006).
- [10] J. K. Stockton, K. Takase, and M. A. Kasevich, Absolute geodetic rotation measurement using atom interferometry, *Phys. Rev. Lett.* 107, 133001 (2011).
- [11] I. Dutta, D. Savoie, B. Fang, B. Venon, C. L. Garrido Alzar, R. Geiger, and A. Landragin, Continuous Cold-Atom Inertial Sensor with 1 nrad/sec Rotation Stability, *Phys. Rev. Lett.* 116, 183003 (2016).
- [12] A. Peters, K. Y. Chung, and S. Chu, A measurement of gravitational acceleration by dropping atoms, *Nature* 400, 849 (1999).
- [13] Z. K. Hu, B. L. Sun, X. C. Duan, M. K. Zhou, L. L. Chen, S. Zhan, Q. Z. Zhang, and J. Luo, Demonstration of an ultrahigh-sensitivity atom-interferometry absolute gravimeter, *Phys. Rev. A* 88, 043610 (2013).
- [14] S. Dimopoulos, P. W. Graham, J. M. Hogan, and M. A. Kasevich, Testing general relativity with atom interferometry, *Phys. Rev. Lett.* 98, 111102 (2007).
- [15] S. Dimopoulos, P. W. Graham, J. M. Hogan, and M. A. Kasevich, General relativistic effects in atom interferometry, *Phys. Rev. D* 78, 042003 (2008).
- [16] D. Aguilera et al., STE-QUEST-test of the universality of free fall using cold atom interferometry, *Class. Quantum Grav.* 31, 115010 (2014).
- [17] S. Dimopoulos, P. W. Graham, J. M. Hogan, M. A. Kasevich, and S. Rajendran, Atomic gravitational wave interferometric sensor, *Phys. Rev. D* 78, 122002 (2008).
- [18] J. M. Hogan, D. M. S. Johnson, S. Dickerson, T. Kovachy, A. Sugarbaker, S. W. Chiow, P. W. Graham, M. A. Kasevich, B. Saif, S. Rajendran, P. Bouyer, B. D. Seery, L. Feinberg, and R. Keski-Kuha, An atomic gravitational wave interferometric sensor in low earth orbit (AGIS-LEO), *Gen. Relativ. Gravit.* 43, 1953 (2011).
- [19] P. W. Graham, J. M. Hogan, M. A. Kasevich, S. Rajendran, New method for gravitational wave detection with atomic sensors, *Phys. Rev. Lett.* 110, 171102 (2013).
- [20] W. Chaibi, R. Geiger, B. Canuel, A. Bertoldi, A. Landragin, and P. Bouyer, Low frequency gravitational wave detection with ground-based atom interferometer arrays, *Phys. Rev. D* 93, 021101 (2016).
- [21] J. M. McGuirk, M. J. Snadden, and M. A. Kasevich, Large area light-pulse atom interferometry, *Phys. Rev. Lett.* 85, 4498 (2000).
- [22] H. Muller, S. Chiow, Q. Long, S. Herrmann, and S. Chu, Atom Interferometry with up to 24-Photon-Momentum-Transfer Beam Splitters, *Phys. Rev. Lett.* 100, 180405 (2008).
- [23] S. W. Chiow, T. Kovachy, H. C. Chien, and M. A. Kasevich, $102\hbar k$ Large area atom interferometers, *Phys. Rev. Lett.* 107, 130403 (2011).
- [24] T. Kovachy, P. Asenbaum, C. Overstreet, C. A. Donnelly, S. M. Dickerson, A. Sugarbaker, J. M. Hogan, and M. A. Kasevich, Quantum superposition at the half-metre scale, *Nature*, 528, 530 (2015).
- [25] K. Kotru, D. L. Butts, J. M. Kinast, and R. E. Stoner, Large-area atom interferometer with frequency-swept Raman adiabatic passage, *Phys. Rev. Lett.* 115, 103001 (2015).
- [26] T. Leveque, A. Gauguier, F. Michaud, F. Pereira Dos Santos, and A. Landragin, Enhancing the area of a Raman atom interferometer using a versatile double-diffraction technique, *Phys. Rev. Lett.* 103, 080405 (2009).
- [27] E. Giese, A. Roura, G. Tackmann, E. M. Rasel, and W. P. Schleich, Double Bragg diffraction: A tool for atom optics, *Phys. Rev. A* 88, 053608 (2013).
- [28] P. Berg, S. Abend, G. Tackmann, C. Schubert, E. Giese, W. P. Schleich, F. A. Narducci, W. Ertmer, and E. M. Rasel, Composite-light-pulse technique for high-precision atom interferometry, *Phys. Rev. Lett.* 114, 063002 (2015).
- [29] i.e., the atoms are prepared in a superposition state by the first Raman pulse ($\Omega_1\tau_1 = \pi/2$), and they are recombined by the second pulse ($\Omega_2\tau_2 \neq \pi/2$). $\Omega_j\tau_j = \pm\pi/2$ are defined as $\pm\pi/2$ pulses for the j th interactions.
- [30] R. B. Li, P. Wang, H. Yan, J. Wang, and M. S. Zhan, Magnetic field dependence of coherent population transfer by the stimulated Raman transition, *Phys. Rev. A*, 77, 033425 (2008).
- [31] K. Wang, Z. W. Yao, R. B. Li, S. B. Lu, X. Chen, J. Wang, and M. S. Zhan, A hybrid wide band low phase noise scheme for Raman lasers in atom interferometry by integrating acousto-optic modulator and feedback loop, *Appl. Opt.*, 55, 989 (2016).
- [32] The angle of polarization rotation is 2 times as the angle of polarization axis of the wave plate rotated, $\beta_2 = 2\beta'_2$.
- [33] K. Usami, and M. Kozuma, Observation of a topologi-

- cal and parity-dependent phase of $m=0$ spin state, Phys. Rev. Lett., 99, 140404 (2007).
- [34] A. Takahashi, H. Imai, K. Numazaki, and A. Morinaga, Phase shift of an adiabatic rotating magnetic field in Ramsey atom interferometry for $m=0$ sodium-atom spin states, Phys. Rev. A, 80, 050102(R) (2009).
 - [35] J. M. Robbins and M. V. Berry, A geometric phase for $m = 0$ spins, J. Phys. A, 27, L435 (1994)
 - [36] N. F. Ramsey, A molecular beam resonance method with separated oscillating fields, Phys. Rev. 78, 695 (1950).
 - [37] C. J. Borde, C. Salomon, S. Avrillier, A. Van Lerberghe, C. Breant, D. Bassi, and G. Scoles, Optical Ramsey fringes with traveling waves, Phys. Rev. A 30, 1836 (1984).
 - [38] J. Bateman, and T. Freearge, Fractional adiabatic passage in two-level systems: Mirrors and beam splitters for atomic interferometry, Phys. Rev. A 76, 013416 (2007).
 - [39] K. Kotru, J. M. Brown, D. L. Butts, J. M. Kinast, and R. E. Stoner, Robust Ramsey sequences with Raman adiabatic rapid passage, Phys. Rev. A 90, 053611 (2014).
 - [40] R. Wynands, A. Nagel, S. Brandt, D. Meschede, and A. Weis, Selection rules and line strengths of Zeeman-split dark resonances, Phys. Rev. A 58, 196 (1998).
 - [41] R. B. Li, L. Zhou, J. Wang, and M. S. Zhan, Measurement of the quadratic Zeeman shift of ^{85}Rb hyperfine sublevels using stimulated Raman transitions, Opt. Commun., 282, 1340 (2009).
 - [42] Each pulse is composed of a pair Raman lasers, and the phase difference of two lasers is zero when their polarizations are simultaneously rotated.
 - [43] P. Cheinet, B. Canuel, F. Pereira Dos Santos, A. Gaudet, F. Leduc, A. Landragin, Measurement of the sensitivity function in time-domain atomic interferometer, IEEE T. Instrum. Meas. 57, 1141 (2008)
 - [44] i.e., the polarizations of Raman lasers can be half-rotated by a fast electro-optical modulator (several nanoseconds).